JOURNAL OF MATERIALS SCIENCE 22 (1987) 4144–4152

Crystallization of Fe–Si–B metallic glasses studied by X-ray synchrotron radiation

W. MINOR
Institute of Experimental Physics, University of Warsaw, Hoza 69, 00-681 Warsaw, Poland

B. SCHÖNFELD*
HASYLAB/DESY, 2000 Hamburg 52, FRG

B. LEBECH, B. BURAS
Physics Department, Risø National Laboratory, DK-4000 Roskilde, Denmark

W. DMOWSKI
Technical University of Warsaw, Narbutta 85, 02-524 Warsaw, Poland

We have studied the crystallization kinetics of $Fe_{90-x}Si_xB_{10}$ amorphous alloys with x ranging from 7 to 21, by synchrotron X-ray radiation. Using energy-dispersive X-ray diffraction, the kinetics of the different crystalline phases evolving during isothermal annealing were followed. These crystalline phases were identified as precipitation of α-Fe(Si) and/or Fe_3Si in the amorphous matrix. At a later time or at a higher temperature, Fe_2B starts to crystallize ($x < 21$). Only at low iron concentration ($x = 21$) was the second phase different, namely Fe_5SiB_2. The hypo- and hyper-eutectic Fe–Si–B glasses were found to crystallize differently. The crystallization processes are discussed in some detail.

1. Introduction

Metallic glasses have attracted much interest due to their remarkable magnetic and mechanical properties [1]. Because the amorphous state is metastable it can be transformed to the stable crystalline state by annealing, performed by increasing the temperature of the metallic glass. During this transformation the magnetic and mechanical properties have been found to deteriorate. Thus a detailed knowledge of the kinetics of the annealing process is a prerequisite for any technological application.

The crystallization of metallic glasses has been investigated by various methods such as differential scanning calorimetry (DSC), transmission electron microscopy, Mössbauer spectroscopy, measurements of coercivity, saturation magnetization and electrical resistivity (for summaries see Köster and Herold [2] and Scott [3]). In most of these methods, the occurrence of a phase change is observed via an anomaly in the data (e.g. by a sudden drop in resistivity), whereas phase identification and kinetic studies of the evolving phases are more difficult. One of the more direct methods for studies of phase transformation is X-ray diffraction, allowing the determination of the structures of each crystalline phase evolving during annealing. However, due to the relatively low intensity of X-rays from conventional X-ray generators such diffraction measurements require long exposure times. This makes time-resolved studies of phase transformations very difficult, and in practice only slow transformations are accessible.

The high intensity of X-rays from synchrotron radiation sources combined with the technique of energy-dispersive X-ray diffraction (EDXD) enables a fast identification of simple crystallographic structures [4], and thus may be used for studies of crystallization kinetics with a time resolution of several minutes. The main aim of this paper is to demonstrate the possibilities given by the X-ray energy-dispersive diffraction and synchrotron radiation for studies of the time dependence of the crystallization process. This will be illustrated by examples of crystallization studies of metallic glasses of the type $Fe_{90-x}Si_xB_{10}$ (for $x = 7$, 11, 15, 18 and 21). Recently, an equivalent neutron scattering technique has been used to study the crystallization process in Fe–P–C amorphous alloys [5].

2. Experimental details

2.1. The samples and the experimental set-up

Amorphous ribbons of $Fe_{90-x}Si_xB_{10}$ with x ranging from 7 to 21 were produced from the constituent elements of at least 99.9 at % purity by the melt-spinning technique. These ribbons, about 20 μm thick and several millimetres wide, were used as samples.

The measurements were made using the X-ray energy-dispersive diffractometer at the storage ring DORIS at HASYLAB/DESY in Hamburg, FRG (for a description see Staun Olsen *et al.* [6]). Diffraction patterns were recorded up to about 60 keV photons, which for the geometry used in the present case ($2\theta_0 = 20.76°$) corresponds to a scattering vector $q = 4\pi \sin\theta_0/\lambda \simeq 110\,\text{nm}^{-1}$.

* *Present address*: Institute of Applied Physics, ETH-Hönggerberg, 8093 Zürich, Switzerland.

0022–2461/87 $03.00 + .12 © *1987 Chapman and Hall Ltd.*

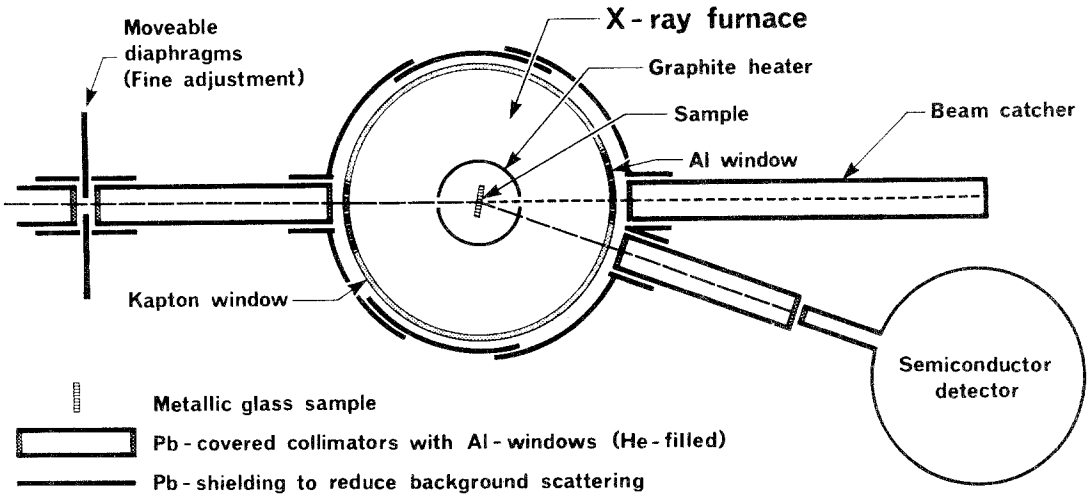

Figure 1 Schematic drawing of the experimental set-up (not to scale).

The incident beam was trimmed by a 200 μm × 200 μm slit to obtain an optimum peak-to-background ratio. A vertical 100 μm slit in front of the detector allowed an overall divergence of 0.8 minutes of arc. A fixed scattering angle $2\theta_0 = 20.76° \pm 0.02°$ was chosen and checked several times during the experiment by measuring the diffraction pattern from a zinc foil placed at the position of the amorphous sample. The scattering angle was sufficiently small to cover a large range in reciprocal space, but large enough to avoid an increase of the width of the peaks occurring at lower Bragg angles [7].

The diffracted radiation was energy-resolved by means of a germanium detector with an energy resolution of 270 eV full width at half height for 17.5 keV photons. For $2\theta_0 = 20.76°$, these photons correspond to a scattering vector $q = 32\,\text{nm}^{-1}$. Because of the well-defined geometrical collimation, the relative scattering vector resolution was governed only by the relative energy resolution of the detector, i.e. $\Delta q/q \simeq \Delta E/E = 0.015$ for 17.5 keV photons. The dead time of the detector system was less than 10%. The detector was coupled to a multichannel pulse height analyzer (2048 channels, set to 30 eV per channel). The recorded diffraction data were transferred from the multichannel analyzer to a PDP-11(03) computer which was used for the preliminary data processing.

The samples were mounted in symmetric transmission geometry in a vacuum furnace [8] which was placed at the diffractometer. The diffraction patterns were contaminated by scattering from the graphite heating element surrounding the sample. In order to minimize this contamination, the heating element is designed so that the incident white beam passes through a slit in the heating element and only the diffracted beam passes through the 0.3 mm thick graphite heating element (Fig. 1) The temperature was controlled and measured by chromel–alumel thermocouples. Whereas the temperature stability was better than 1° C during measurements on each sample, an absolute calibration of the thermocouples used, performed after the experiment, showed deviations ΔT of up to 5° C for the temperature range of interest, when compared to the standard tables for chromel–alumel thermocouples. Because ΔT for the chromel–alumel thermocouples was found to depend on the number of times the thermocouples had been cycled above 700° C, the temperatures quoted in the following have not been corrected for this deviation. Hence, the temperatures quoted are nominal temperatures, correct only to within 5° C.

For each sample a series of diffraction patterns was collected at different times counted from the moment in which the sample reached the desired temperature for isothermal annealing. This temperature was reached from room temperature in about 10 min, a time which is much shorter than the time needed to reach saturation of the crystallization process of the samples. In Table I we have listed the compositions of the samples, the temperatures at which isothermal annealing was studied, the time needed to reach saturation of a particular crystallization stage and the crystalline phases obtained. The applied annealing temperatures in the range from 350 to 462° C are lower than those found for the onset of crystallization using the DSC technique at constant heating rate [9]. The reason is presumably the slow heating rate used in the present experiment to bring the sample from room temperature to the desired temperature in the prescribed time. A dependence of annealing temperature on heating rate has been observed in several cases, for instance by Decristofaro *et al.* [10]. They studied an $Fe_{82}Si_8B_{10}$ sample by the DSC technique and found that changing the heating rate from 20 to 5° C min^{-1} decreased the onset of crystallization by 50° C.

2.2. Evaluation of diffraction patterns

The measuring times were 200 to 500 sec for a complete energy-dispersive X-ray diffraction pattern with sufficient statistics. In view of that, a rather low annealing temperature was chosen in order to obtain a corresponding crystallization rate. The intensity of the radiation emitted by a storage ring decreases with time (it is proportional to the electron current). Thus, in order to evaluate the time-dependence of the crystallization, normalization of each diffraction pattern is required. The normalization was done using the intensity of the Fe$K\alpha$-fluorescence line, but also checked by normalizing to the electron current. Both

TABLE I Summary of the results of the diffraction data and the analysis of the crystallization kinetics.

Composition	Sample No.	Annealing temperature (°C)	Time for reaching 0.95 V ($t = \infty$) (min)	Phases of Stage 1	Phases of Stage 2	n (X-ray)*	n (DSC)†
Hypoeutectic $Fe_{90-x}Si_xB_{10}$ alloys ($x < 14$)							
$Fe_{83}Si_7B_{10}$	1	350	450	α-Fe(Si)		1.3 ± 0.1	
		438	200		α-Fe(Si)‡	2.9 ± 0.1	
							2.5 ± 0.2
			200		Fe_2B	2.2 ± 0.4	
	2	379	40	α-Fe(Si)		1.1 ± 0.1	
	3	386	110	α-Fe(Si)		0.8 ± 0.1	
$Fe_{79}Si_{11}B_{10}$	4	414	110	Fe_3Si–α-Fe(Si)		1.5 ± 0.2	
			2100		Fe_3Si–α-Fe(Si)	1.9 ± 0.4	2.3 ± 0.2
			2100		Fe_2B	1.4 ± 0.3	
Hypereutectic $Fe_{90}Si_xB_{10}$ alloys ($x > 14$)							
$Fe_{75}Si_{15}B_{10}$	5	438	1000	Fe_3Si		2.0 ± 0.3	
							2.7 ± 0.2
			1400	Fe_2B		1.2 ± 0.3	
$Fe_{72}Si_{18}B_{10}$	6	426	900	Fe_3Si		1.9 ± 0.3	
	7	438	600	Fe_3Si		1.2 ± 0.1	
							2.9 ± 0.2
			1600	Fe_2B		1.0 ± 0.1	
	8	462	140	Fe_3Si		1.1 ± 0.1	
			280	Fe_2B		0.9 ± 0.1	
$Fe_{69}Si_{21}B_{10}$§	9	426	900	Fe_3Si, Fe_5SiB_2		2.7 ± 0.2	
	10	438	350			3.3 ± 0.3	
	11	450	90			3.6 ± 0.3	
	12	461	50			3.0 ± 0.2	

*This work.
† Estimated from Fig. 2 in Zaluska and Matyja [20]. The n values quoted are in rough agreement with the n values obtained by Zaluska and Matyja, private communication, 1984.
‡ Annealing temperature increased to 438° C after 1375 min at 350° C.
§ The n values and the times for reaching 0.95 V ($t = \infty$) are for Fe_3Si.

normalizations were in good agreement. The integrated intensities of selected reflections were determined from fits to the background (polynomials up to the fourth order) and assuming a Gaussian shape of the reflections [11]. This procedure was critical, in particular for the weaker reflections developing during crystallization and located on the strongly modulated background characteristic of the amorphous sample and the white-beam energy-dispersive method. The phase identification was done by inferring the crystal structures from the lattice spacings. The latter were calculated from the positions of the reflections using the Bragg equation for the energy dispersive method

$$Ed \sin \theta_0 = \tfrac{1}{2} hc = 0.6199\,\text{keV nm} \quad (1)$$

where E is the photon energy, h Planck's constant and c the velocity of light. Very useful has also been the comparison of the lattice parameters of the assumed structure with those which may conceivably be products of the amorphous-to-crystalline transformation of Fe–Si–B (Table II). A semi-quantitative assessment of the integrated intensities of the main reflections was also taken into account in the phase identification. The time-dependence of the crystallization of a given

TABLE II Some crystal structures of crystalline compounds and alloys that could conceivably be products of the amorphous-to-crystalline transformation of Fe–Si–B alloys

Phase	Crystal system	Space group	Lattice constants (nm)
α-Fe(Si)*	Cubic	Im3m	$a = 0.28662$ to 0.28133†
Fe_3Si	Cubic	Fm3m	$a = 0.56554$‡
FeB	Orthorombic	Pnma	$a = 0.5506$, $b = 0.2952$, $c = 0.4061$‡
Fe_2B	Tetragonal	I4/mcm	$a = 0.5109$, $c = 0.425$‡
Fe_3B	Tetragonal	$I\bar{4}$	$a = 0.864$, $c = 0.428$§
Fe_5Si_3	Hexagonal	P6/mcm	$a = 0.67552$, $c = 0.47174$‡
Fe_5SiB_2	Tetragonal	I4/mcm	$a = 0.543$, $c = 1.033$¶

*The notation α-Fe(Si) used here and in the text is a solid solution of x at % Si in α-Fe.
† The lattice parameter of α-Fe(Si) depends on the amount ($0 \leqslant x \leqslant 31$ at %) of dissolved silicon (see Farquhar *et al.* [14]).
‡ See Pearson [25].
§ See Köster and Herold [2].
¶ See Aronsson and Engström [26].

phase follows directly from the time-dependence of the integrated intensities of the observed reflections characteristic for the phase.

2.3. Analysis of the time-dependence of crystallization

In Section 3 the time-dependence of the crystallization is presented on the basis of one of the models of isothermal transformation kinetics. A review of such models was recently published by Christian [12]. Below we briefly mention a few points relevant to our studies.

The time-dependence of crystallization is usually described by the Avrami equation

$$\xi = 1 - \exp[-K(t - t_0)^n] \quad (2)$$

Here ξ is the volume fraction $V(t)/V(t = \infty)$ of the transformed phase at time t, t_0 the incubation time for onset of crystallization, K the rate constant of the transformation which follows the Arrhenius law, and n the Avrami exponent. Equation 2 was proposed by Avrami [13–15] for interface-controlled transformation, assuming that only one nucleation and growth process is involved and that random nucleation is present. The diffusion-controlled transformation is more complex and has been treated by Wert and Zener [16] and Ham [17]. The application of the Avrami equation for the description of the time-dependence of crystallization is at present a matter of discussion (see for instance [18]). Therefore, we have used the Avrami equation mainly as a convenient expression for fitting our experimental data. We refrain, however, from drawing detailed conclusions on the basis of the values obtained for the Avrami exponent n. This is in conformity with the main aim of this paper (see Section 1). Nevertheless, although we treat n as a fitting parameter, a few comments on the n values to be expected from a crystallization study seem relevant. Here we follow Ramanan and Fish [19] who express n by

$$n = a + bp \quad (3)$$

where a refers to the nucleation rate and varies between 0 and 1, b takes the values 1, 2 and 3 and represents the dimensionality of the crystal growth, and p defines the mechanism that controls the crystal growth: $p = 0.5$ for diffusion-controlled growth (parabolic in time) and $p = 1$ for interface-controlled growth (linear in time). This means that for a three-dimensional growth process, n may take values between 1.5 and 3 for quenched-in nuclei ($a = 0$) and between 2.5 and 4 for a constant nucleation rate ($a = 1$).

3. Experimental results

3.1. Identification of crystalline phases

Examples of EDXD diffraction patterns illustrating the development of crystallization are shown in Figs 2 and 3. The intensities are shown on a logarithmic scale. For clarity the diffraction patterns have been displaced vertically with respect to each other.

Fig. 2a shows the results of annealing $Fe_{83}Si_7B_{10}$ (Sample 1) at 350° C. As can be seen, pronounced crystallization evolves with time. However, an amorphous matrix is still present after 1375 min annealing. The evolving structure was identified as a bcc structure, a solid solution of silicon in α-Fe (labelled α-Fe(Si)). Fig. 2b shows the same sample when we raise the temperature and anneal the sample further at 438° C. The already present crystalline phase α-Fe(Si) increases in volume and a new phase – identified as tetragonal Fe_2B (see Table II) – appears. The amorphous background is greatly reduced. Fig. 3 shows the results of annealing $Fe_{72}Si_{18}B_{10}$ (Sample 7) at 438° C. During annealing for about 150 min only one phase evolves, identified as Fe_3Si – an ordered fcc structure (see Table II). At longer annealing time a second phase appears. This phase could be identified as Fe_2B.

The crystallization processes of several samples of $Fe_{90-x}Si_xB_{10}$ were studied in detail. Five different compositions ($7 \leqslant x \leqslant 21$) were available and the different crystalline phases evolving during crystallization were derived from the diffraction patterns as described in Section 2.2. The results of the phase identification are summarized in the fifth and sixth columns of Table I. Inspection of Table I shows that with the exception of Samples 2, 3 and 6 several phases crystallize during isothermal annealing (see also Figs 4, 5 and 6 below). For a small silicon concentration ($x = 7$) the first phase to crystallize is a solid solution of silicon in α-Fe (α-Fe(Si)). For large silicon concentration ($11 < x \leqslant 21$) the first phase to crystallize is Fe_3Si. For intermediate silicon concentrations ($x = 11$) the first phase to crystallize is a mixture of α-Fe(Si) and Fe_3Si (labelled Fe_3Si–α-Fe(Si)). The second phase to crystallize is Fe_2B for $7 \leqslant x \leqslant 18$ and Fe_5SiB_2 for $x = 21$.

As mentioned, only one crystalline phase was observed in Samples 2, 3 and 6. However, it should be noticed that the annealing temperatures of Samples 2 and 3 were lower (379 and 386° C, respectively) than the annealing temperature of Sample 1 (438° C), leading to the appearance of the second crystalline phase. A similar comment can be made when comparing Sample 6 with Samples 7 and 8. Thus, it seems justified to state that for all the concentrations studied by us, more than one crystalline phase can evolve during isothermal annealing at an appropriate temperature.

3.2. Kinetic studies

Figs 4 to 7 show, as illustrative examples, the time-dependences of the integrated intensities of selected Bragg reflections for some compositions and different annealing temperatures. The intensities are presented on a relative scale.

As illustrated for example by $Fe_{83}Si_7B_{10}$ annealed at 350° C (Figs 2a and 4), one notices that at the beginning the crystallization process is fast. Afterwards it slows down and reaches 95% of its saturation value after about 450 min. After 1375 min annealing at 350° C, the temperature of this sample was increased to 438° C (Figs 2b and 4) and the annealing continued. At this elevated temperature the crystalline α-Fe(Si) phase developed at 350° C increased in volume. About 60 min after the increase of temperature a new phase (Fe_2B) started crystallizing. Both α-Fe(Si) and Fe_2B

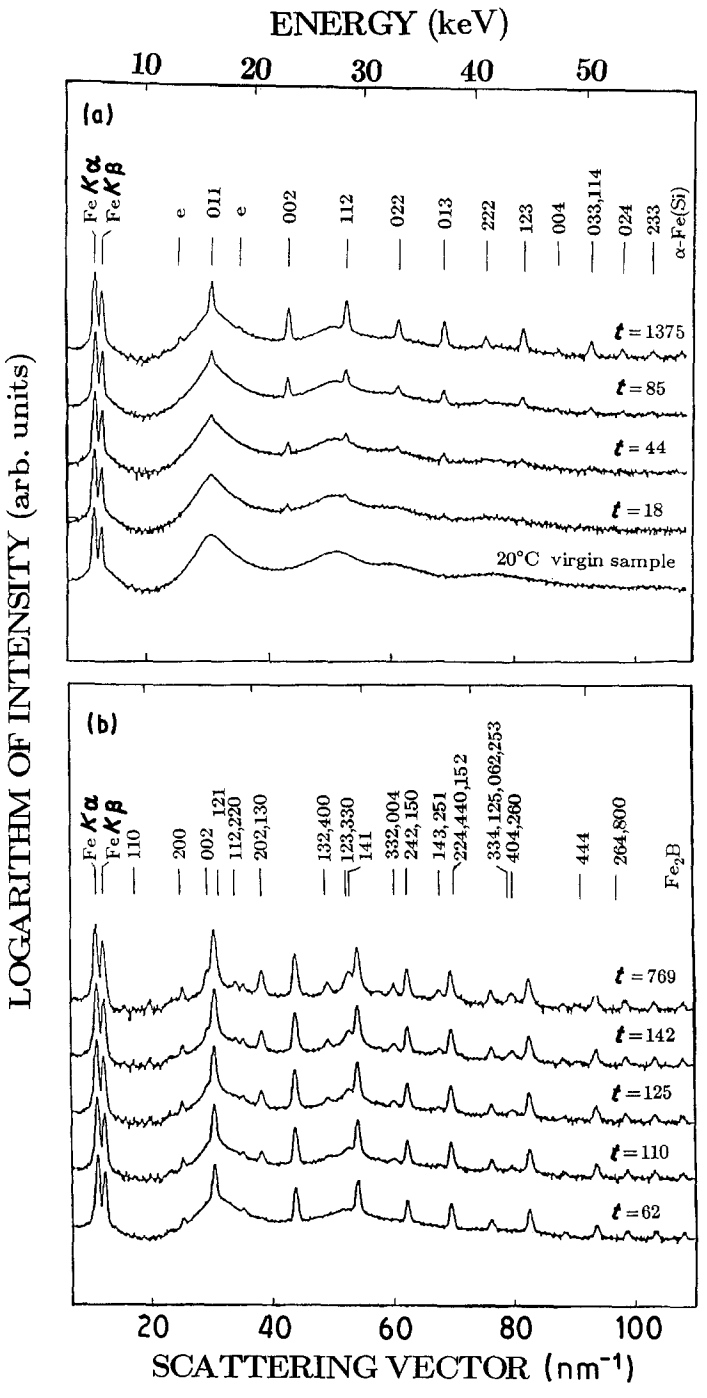

Figure 2 Series of diffraction patterns of the crystallization of $Fe_{83}Si_7B_{10}$: (a) the amorphous sample after annealing at 350° C for 18, 44, 85 and 1375 min, (b) the same sample after additional annealing at elevated temperature (438° C) for 62, 110, 125, 142 and 769 min, respectively. In (a) is also shown the pattern for the amorphous virgin sample at room temperature.

reached saturation after 200 additional minutes at 438° C. Two other samples of the same composition were annealed at 379 and 386° C. Here only α-Fe(Si) developed during the measuring times of 300 and 900 min, respectively.

Inspection of Fig. 5 clearly shows that for $Fe_{79}Si_{11}B_{10}$ and an isothermal annealing temperature above 400° C, crystallization takes place in two stages: Fe_3Si–α-Fe(Si) crystallizes first and Fe_2B crystallizes at a later time. The crystallization of Fe_2B is accompanied by further crystallization of Fe_3Si–α-Fe(Si). For $Fe_{75}Si_{15}B_{10}$ (Fig. 6) only one stage of crystallization of Fe_3Si and Fe_2B was observed. In Fig. 7 we show the time-dependence of the integrated intensities of some Bragg peaks of the Fe_3Si phase developing during annealing of $Fe_{69}Si_{21}B_{10}$ at different annealing temperatures, T_a. These data were used to make the time–temperature–transformation (TTT) diagram shown in Fig. 8. If we assume that the crystallization process is the same at room temperature and elevated temperatures, we may extrapolate the data shown in Fig. 8 to room temperature. In this way we estimate that at room temperature, asymptotic and 10% crystallization of the Fe_3Si phase in $Fe_{69}Si_{21}B_{10}$ would be reached after 10^{20} and 10^{17} years, respectively.

In order to gain some insight into the crystallization processes we have fitted our kinetic data for all samples investigated to the Avrami equation (Equation 2). As already mentioned the integrated intensity of a reflection is proportional to the volume of the sample and thus $V(t)$ and $V(t = \infty)$ in Equation 2 can be replaced by the respective integrated intensities. The kinetics of the crystallization of a particular phase were studied directly by analysis of the time-dependence of the integrated intensities of the Bragg peaks. The parameters of the Avrami equation, n, K and t_0, were found at a fixed annealing temperature by a least-squares fit to the experimental data for each

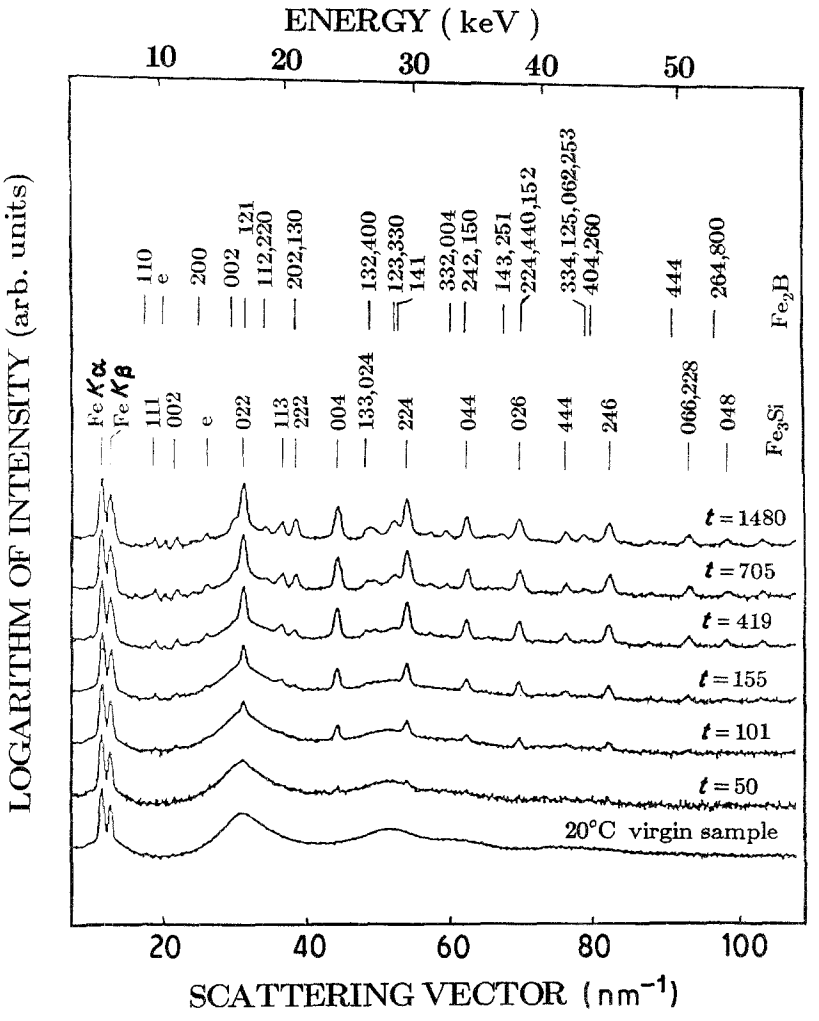

Figure 3 Series of diffraction patterns of the crystallization of $Fe_{72}Si_{18}B_{10}$ during annealing at 438° C for 50, 101, 155, 419, 705 and 1480 min. The diffraction pattern of the virgin amorphous sample is also presented.

crystallization step. The seventh column in Table I summarizes the results of such fits. The values of n listed in Table I are average values obtained from fits for different reflections. The solid curves in Figs 4 to 7 show the results of these fits. The errors, Δn, for the n values quoted in Table I are based on the χ^2 obtained in the fits. If only one reflection was used to determine n, Δn reflects the accuracy of the fit. If more than one reflection were included in the fit, Δn reflects the accuracy of the fits and the consistency between the n values determined for each of the reflections.

4. Summary and discussion

A phase diagram of the ternary Fe–Si–B metallic glasses has been given by Ramanan and Fish [19]. From this diagram, we estimate the eutectic point to correspond to $x \simeq 14$ for the $Fe_{90-x}Si_xB_{10}$ amorphous alloys. According to the classification of Ramanan and Fish [19] the hypoeutectic compounds correspond to $x < 14$ (iron-rich) and the hypereutectic compounds to $x > 14$. We have investigated two hypoeutectic compounds ($x = 7$, 11) and three hypereutectic ones ($x = 15$, 18, 21). For all these samples, the

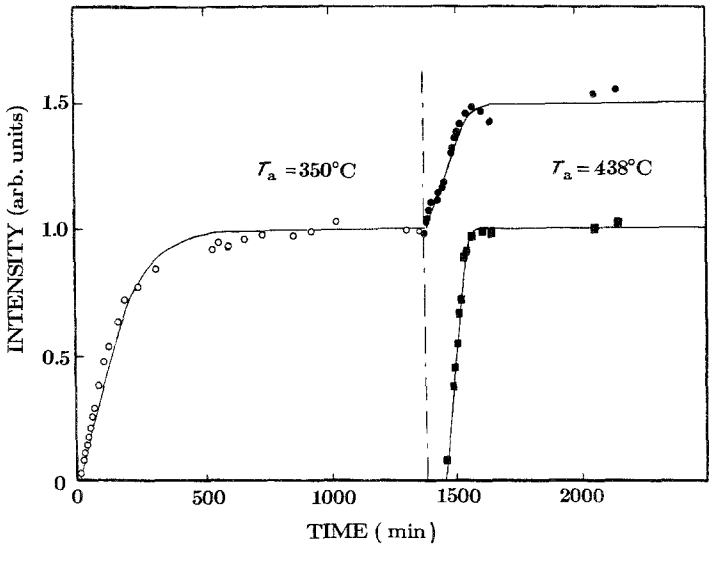

Figure 4 The time-dependence of the integrated intensity of (○, ●) the (0 0 2) peak of α-Fe(Si) and (■) the (0 2 2), (1 3 0) peaks of Fe_2B of $Fe_{83}Si_7B_{10}$ during annealing. The left-hand side of the figure shows annealing at 350° C and the right-hand side shows continued annealing at 438° C. The solid curves represent the least-squares fits to the Avrami equation.

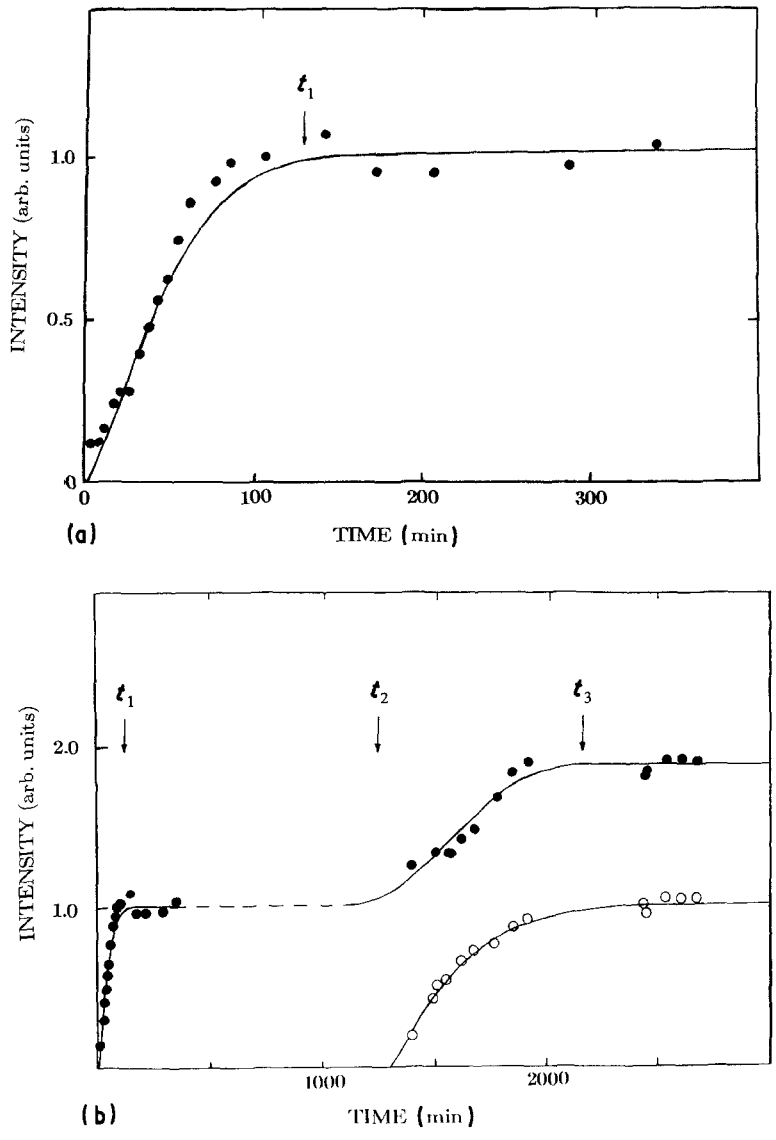

Figure 5 The time dependences of the integrated intensity of (●) the overlapping (0 0 2) α-Fe(Si) and (0 0 4) Fe_3Si peaks of $Fe_{79}Si_{11}B_{10}$ during annealing at 414° C for (a) 300 min and (b) 2600 min. In (b) the time-development of (○) the (0 0 4) + (3 3 2) peak of Fe_2B is also presented. The solid curves represent the least-squares fits to the Avrami equation (see Table I).

diffraction patterns showed crystallization of α-Fe(Si) or Fe_3Si and Fe_2B after isothermal annealing. Only for $Fe_{69}Si_{21}B_{10}$ did we find crystallization of Fe_5SiB_2 instead of Fe_2B.

For the hypoeutectic compounds, we found that the crystallization took place in two stages, in the sense that when crystallizing during isothermal annealing, α-Fe(Si), Fe_3Si or Fe_3Si–α-Fe(Si) appears to saturate at a time t_1 as illustrated in Fig. 5 (first stage of crystallization). At a later time t_2 (or at a higher temperature), Fe_3Si–α-Fe(Si) again starts to crystallize but this time simultaneously with the crystallization of Fe_2B. Both phases then saturate at t_3 (second stage of crystallization, see Fig. 5), and the final level of saturation reached for Fe_3Si–α-Fe(Si) is now higher than that reached at t_2. For the hypereutectic compounds, the first phase crystallizes in one stage only and the second phase starts to develop with some delay (see Fig. 6).

Although there exist a few inconsistencies between

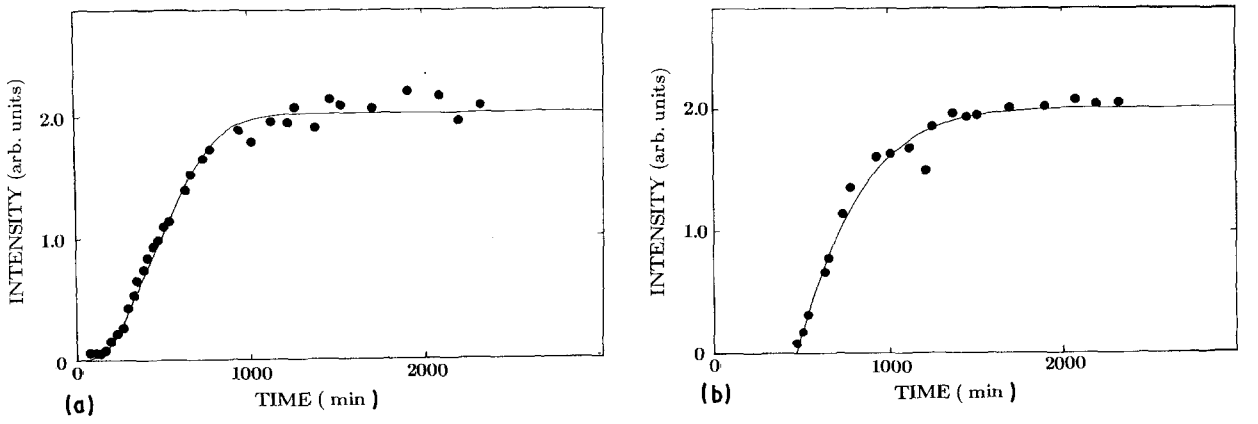

Figure 6 The time-dependence of (a) the (0 0 4) peak of Fe_3Si and (b) the (1 1 2) + (2 2 0) peaks of Fe_2B of $Fe_{75}Si_{15}B_{10}$ alloy during annealing at 438° C for 2300 min. The solid curves represent the least-squares fit to the Avrami equation.

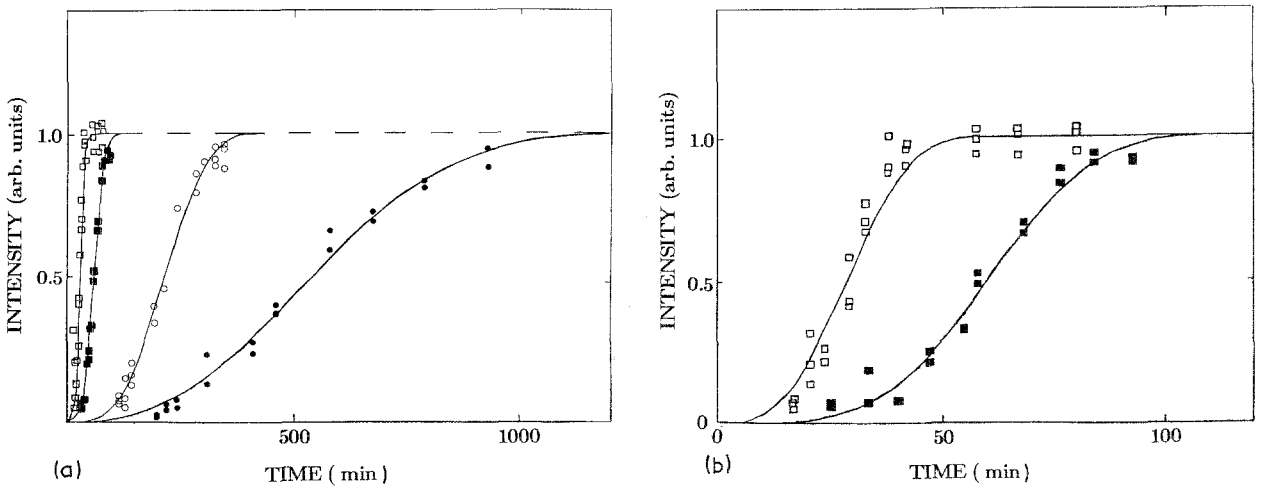

Figure 7 The time-dependence of the integrated intensity of the (0 0 4) Fe_3Si peak during annealing of $Fe_{69}Si_{21}B_{10}$. In (a) at (●) 426, (○) 438, (■) 450 and (□) 461° C. In (b), the results obtained at 450 and 461° C are presented on an expanded time scale. The solid curves represent least-squares fit to the Avrami equation.

our results and the results of other authors, the general features are very similar. In agreement with our data, detailed DSC studies of hypoeutectic $Fe_{90-x}Si_xB_{10}$ glasses show two stages of crystallization for $x = 6, 7$ [20], for $x = 8$ [10] and for $x = 10$ [19]. For the eutectic samples ($x = 14$) Ramanan and Fish [19] find one stage of crystallization in agreement with our results for hypereutectic $Fe_{90-x}Si_xB_{10}$ glasses, whereas Zaluska and Matyja [20] rather surprisingly find three stages of crystallization for $x = 15$.

The crystallization products of Fe–Si–B systems with approximately 10 at % B were discussed in several papers. Ramanan and Fish [19] and Decristofaro *et al.* [10] found α-Fe(Si) and tetragonal Fe_3B. Zaluska and Matyja [21] and Gonser *et al.* [22], using Mössbauer spectroscopy for $x = 10$ and 15, found Fe_3Si–α-Fe(Si) and Fe_2B, in consistency with our findings. $Fe_{69}Si_{21}B_{10}$ was only studied by us. The apparent disagreement between the crystallization products determined by the direct methods (e.g. Mössbauer spectroscopy and diffraction studies) and the DSC may be explained by the fact the Fe_3B is a metastable phase [2] that decomposes into α-Fe and Fe_2B.

The disagreement between the n values of our data and those found when using DSC in the isothermal mode ([10], see Table I) is a consequence of the fact that in the DSC method all phase transformations are observed simultaneously and overlap in time, whereas in the present experiment, crystallization of each phase can be observed separately. Therefore, the n values obtained in the present study are for the individual phases and crystallization stages. From Table I it may be noted that the n values for the Fe_2B phase are always lower than for the Fe_3Si phase. This may be explained first of all by the fact that a certain amount of boron atoms evaporates from the sample if the crystallization takes place under vacuum [23]. Furthermore, the intensities of the Fe_2B diffraction peaks are low, and often overlap with the diffraction peaks from some of the other phases. Therefore, it is more difficult to evaluate the intensities of these peaks accurately. As discussed in Section 2.3, the kinetics of crystallization are determined by the nucleation and growth rate. If one of these processes is slow it determines the net crystallization rate of the whole process. In most cases we found n values between 0.8 and 2.0 for the first stage. This can be explained by the existence of quenched-in nuclei and a diffusion-controlled crystallization (see Equation 3). Only in the case of $Fe_{69}Si_{21}B_{10}$ do the larger n values indicate a constant nucleation rate (see Equation 3).

The present study of the crystallization process in Fe–Si–B metallic glasses, using synchrotron X-rays combined with the energy-dispersive technique,

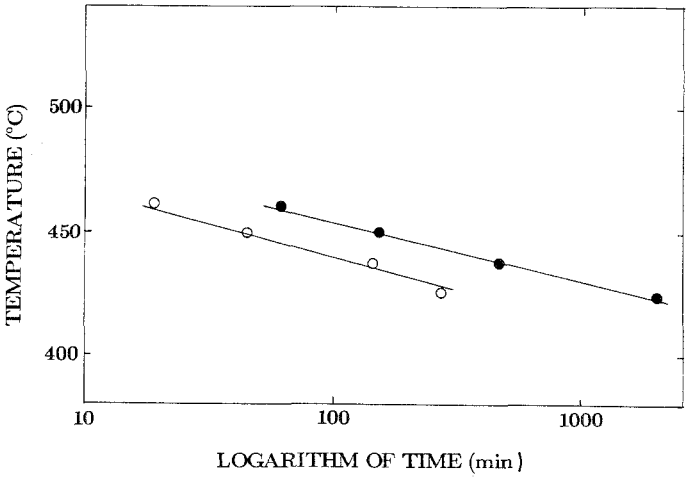

Figure 8 Time–temperature–transformation (TTT) diagram for $Fe_{69}Si_{21}B_{10}$ constructed on the basis of the results presented in Fig. 7; (○) 10%, (●) full crystallization.

illustrates that it is feasible to study time-dependent phenomena with relative short time scales using this technique. For an appropriate choice of scattering geometry a full diffraction pattern may be obtained in a short time. For crystallization studies these patterns will often be complex, because the crystallized matrix contains several compounds, and phase identification is at the moment only possible for simple structures. Also it should be noted that fluorescence lines and escape peaks may in certain cases (especially for heavy atoms) complicate the diffraction pattern, a problem which to some extent may be overcome by changing the scattering angle. Possibly, the best way of studying crystallization processes by diffraction is to use the energy-dispersive method for phase identification, and the angle-dispersive method combined with a position-sensitive detector to study the time-dependence of selected Bragg peaks in each phase.

Acknowledgements

The authors would like to thank D. Juul Jensen, L. Dobrzynski and H. Matyja for stimulating discussions. One of us (W.M.) thanks Risø National Laboratory and HASYLAB/DESY for financial support, and for the support by Contract MR-I-5 at Warsaw University. This work was supported by The Danish Natural Science Research Council.

Recently S. B. Qadri *et al.* [27] has studied the isothermal crystallization of $Fe_{83}B_{17}$ using a similar technique.

References

1. H. BECK and H. -J. GÜNTHERODT, in "Glassy Metals I", edited by H. -J. Güntherodt and H. Beck (Springer, Berlin, 1981) Ch. 1.
2. U. KÖSTER and U. HEROLD, in "Glassy Metals I", edited by H. -J. Güntherodt and H. Beck (Springer, Berlin, 1981) Ch. 10.
3. M. G. SCOTT, in "Amorphous Metallic Alloys", edited by F. E. Luborsky (Butterworths, Borough Green, Kent, UK, 1984) p. 144.
4. B. BURAS, J. STAUN OLSEN and L. GERWARD, *Nucl. Instr. Meth.* **135** (1976) 193.
5. C. TÊTE, M. VERGNAT, G. MARCHAL and Ph. MANGIN, *Solid State Commun.* **53** (1985) 191.
6. J. STAUN OLSEN, B. BURAS, L. GERWARD and S. STEENSTRUP, *J. Phys. E* **14** (1981) 1154.
7. B. BURAS, N. NIMURA and J. STAUN OLSEN, *J. Appl. Crystallogr.* **11** (1978) 137.
8. B. BURAS, B. LEBECH and W. KOFOED, *Rev. Phys. Appl.* **19** (1984) 743.
9. W. DMOWSKI, T. JAGIELINSKI, T. WALECKI and H. MATYJA, *J. Physique* **C8** (1980) 127.
10. N. DECRISTOFARO, A. FREILICH and G. FISH, *J. Mater. Sci.* **17** (1982) 2365.
11. J. LAUTERJUNG, G. WILL and E. HINZE, *Nucl. Instr. Meth. Phys. Res.* **A239** (1985) 281.
12. J. W. CHRISTIAN, "The Theory of Transformations in Metals and Alloys", Part I, 2nd Edn (Pergamon, New York, 1981) p. 564.
13. M. AVRAMI, *J. Chem. Phys.* **7** (1939) 1103.
14. *Idem, ibid.* **8** (1940) 212.
15. *Idem, ibid.* **9** (1941) 177.
16. C. WERT and C. ZENER, *J. Appl. Phys.* **21** (1950) 5.
17. F. S. HAM, *J. Phys. Chem. Solids* **6** (1958) 335.
18. C. W. PRICE, *Scripta Metall.* **19** (1985) 669.
19. V. R. V. RAMANAN and G. E. FISH, *J. Appl. Phys.* **53** (1982) 2273.
20. A. ZALUSKA and H. MATYJA, in Proceedings of 4th International Conference on Rapidly Quenched Metals, Edited by T. Masumoto and L. K. Suzuki, Japan Institute of Metals, Tokyo, 1981, p. 683.
21. *Idem. J. Mater. Sci.* **18** (1983) 2163.
22. U. GONSER, M. GHAFARI, M. ACKERMANN, H. P. KLEIN, J. BAUER and H. -G. WAGNER, in Proceedings of 4th International Conference on Rapidly Quenched Metals, Edited by T. Masumoto and L. K. Suzuki, Japan Institute of Metals, Tokyo, 1981, p. 639.
23. H. -G. WAGNER, M. ACKERMANN and U. GONSER, *J. Non-Cryst. Solids* **61/62** (1984) 847.
24. M. C. FARQUHAR, H. LIPSON and A. R. WEILL, *J. Iron Steel Inst.* **152** (1945) 457.
25. W. B. PEARSON, in "A Handbook of Lattice Spacings and Structures of Metals and Alloys" Vol. 2 (Pergamon, New York, 1958) p. 409, 552.
26. B. ARONSSON and I. ENGSTRÖM, *Acta Chem. Scand.* **14** (1960) 1403.
27. S. B. QADRI, W. T. ELAM, J. D. AYERS, C. L. VOLD, E. F. SKELTON and A. W. WEBB, *Nucl. Instr. and Methods* **A246** (1986) 817.

Received 29 January
and accepted 15 April 1987